2012

A significant improvement in the superconducting properties of MgB2 by co-doping with graphene and nano-SiC

K S B De Silva
University of Wollongong, kaludewa@uow.edu.au

X Xu
University of Wollongong, xun@uow.edu.au

Xiaolin Wang
University of Wollongong, xiaolin@uow.edu.au

D Wexler
University of Wollongong, david_wexler@uow.edu.au

D Attard
University of Wollongong, darrena@uow.edu.au

See next page for additional authors

Available online at www.sciencedirect.com

SciVerse ScienceDirect

Scripta Materialia 67 (2012) 802–805

Scripta MATERIALIA

www.elsevier.com/locate/scriptamat

A significant improvement in the superconducting properties of MgB_2 by co-doping with graphene and nano-SiC

K.S.B. De Silva, X. Xu, X.L. Wang, D. Wexler, D. Attard, F. Xiang and S.X. Dou*

Institute for Superconducting and Electronic Materials, University of Wollongong, Northfields Avenue, Wollongong, NSW 2522, Australia

Received 17 April 2012; revised 22 June 2012; accepted 11 July 2012
Available online 17 July 2012

The effects of graphene (G) and nanosilicon carbide (SiC) co-doping on the superconducting properties of MgB_2 were studied using bulk samples. SiC remains one of the best dopants which can significantly improve the high field performance, while graphene is emerging as a new dopant for MgB_2, which can improve the zero field critical current density (J_c). The superconducting properties characterized by J_c, the intergrain connectivity, and the critical fields were significantly improved by the use of both SiC and graphene as dopants.

Keywords: Metallic superconductors; Co-doping; Transmission electron microscopy; Electrical properties

Due to the high critical temperature (T_c) of 40 K, intrinsically "weak link" free grain boundaries, and low fabrication cost MgB_2 is believed to be promising to replace conventional low T_c superconductors in many cryogen-free applications, such as magnetic resonance imaging, cavities, flying wheels, high field magnets, etc. For practical applications that require carrying large supercurrents in the presence of a magnetic field improvements in the critical current density (J_c) have been the key research topic for MgB_2. So far extensive research has been undertaken to enhance the superconducting properties, such as the critical current density (J_c), upper critical field (H_{c2}) and irreversibility field (H_{irr}). A significant improvement in J_c field dependence is one of the most important factors permitting its usage in industrial applications. Chemical doping has been identified as the simplest and cheapest way to improve the electronic structures of superconductors and their superconducting properties. In particular, carbon-containing dopants, including silicon carbide (SiC), nanocarbon, carbon nanotubes (CNTs), hydrocarbon/carbohydrate composites, graphite and graphene are effective means to improve the J_c field dependence and H_{c2} [1–9].

Among all the dopants SiC appears to be the most effective, resulting in a high density of micro-structural defects, favouring superior improvements in the superconducting properties compared with other carbon or carbon-based dopants [1]. However, as in many carbon dopants, SiC also has an adverse effect on J_c in the low field region. On the other hand, graphene is a dopant which can improve J_c in the low field region, through improved inter-grain connectivity [8–10]. In this work we report success with a significant improvement in J_c in both low and high fields in MgB_2 with co-doping of graphene and nano-SiC. Our finding paves the way for MgB_2 to be useful in both high and low field applications.

Graphene and SiC co-doped bulk samples were prepared via a diffusion method from crystalline boron powder (99.999% pure, 0.2–2.4 μm), Mg powder (99% pure, 352 mesh), SiC (99% pure, <30 nm) and highly reduced chemically converted graphene (rCCG) as precursors. The detailed chemical synthesis of rCCG has been described in a previous work [9]. Initially boron and graphene powders were mixed at a weight ratio of MgB_2:graphene:SiC equal to 1:0.025:x, where $x = 0$, 5, or 7.5 wt.% SiC. The weight ratio of graphene was kept constant at 2.5 wt.% for co-doped samples, as this gave the optimum results in a previous work [8]. Powders were then pressed into pellets 13 mm in diameter and inserted into a soft iron tube at a stoichiometric ratio of Mg to B, plus excess Mg to compensate for the loss of Mg during sintering. The samples were sintered at 800 °C for 10 h in a quartz tube at a heating rate of 5 °C min^{-1} in high purity argon gas (99.9% Ar). The phase identification and crystal structure investigations

* Corresponding author; e-mail: shi@uow.edu.au

1359-6462/$ - see front matter © 2012 Acta Materialia Inc. Published by Elsevier Ltd. All rights reserved.
http://dx.doi.org/10.1016/j.scriptamat.2012.07.014

were carried out using an X-ray diffractometer (GBCMMA) with Cu K_α radiation ($\lambda = 1.54059$ Å). A JEOL JSM-7500FA field emission scanning electron microscope equipped with an ultra-thin window (UTW) JEOL hyper-minicup energy dispersive spectrometer was used for scanning electron microscopy (SEM) analysis. Transmission electron microscopy (TEM) was performed on powders using a JEOL 2011 200 keV analytical instrument. The superconducting transition temperature T_c was determined from the a.c. susceptibility measurements, and the magnetic J_c value was derived from the width of the magnetization loop using Bean's model [11] using a physical properties measurement system. The resistivity measurements were conducted using the standard d.c. four probe technique under magnetic fields up to 13 T. The upper critical field (H_{c2}) and the irreversibility field (H_{irr}) were determined using the 90% and 10% criteria of $R(T)$ for different applied fields, where $R(T)$ is the normal state resistance near 40 K. The active cross-section (A_F) was calculated from the resistivity ρ from Rowell's model [12].

According to the XRD patterns (Fig. 1a) the dominant phase within all the samples was MgB_2. As the SiC doping level increased Mg_2Si and unreacted SiC peaks can be seen with more pronounced peak intensities [13]. Figure 1b–f shows the field emission scanning electron microscopy (FESEM) backscattered images for doped and co-doped samples. There are four distinct grey scale intensities present in the images, with the backscattered images showing increasing brightness with atomic number. Region 1 is the darkest phase, indicating that it has the lowest relative atomic number. This phase is present at all levels of doping, and increases with the amount of SiC and graphene doping. EDS analysis confirmed the presence of Mg and B only in this phase (B-rich phase). Region 2 shows a lighter grey scale than region 1, indicating a higher relative atomic number. EDS confirmed the presence of Mg and B only, however with a higher Mg:B ratio being responsible for the increased grey scale intensity. The area fraction of region 2 increases with the doping level and always shows a higher area fraction than region 1. Region 3 is the most prominent phase in all samples, however, the relative amount decreases with the level of doping. EDS analysis of this area confirmed the presence of Mg, B, C, O and Si. Region 4 shows the brightest grey scale level, indicating that this phase has the highest relative atomic mass. EDS analysis confirmed the presence of Mg, B, C, O and Si, with significantly higher Si and O concentrations. The relative amount of this phase increased with the level of SiC doping. From the above observations it is clear that the addition of SiC contributes to the formation of Mg_2Si and B-rich phases, which has a favourable effect on improving flux pinning due to the formation of normal superconducting interfaces [14]. Figure 1d, is an enlarged view of the area circled in Figure 1e, which reveals the fine distribution of region 4 in the main MgB_2 matrix.

Preliminary TEM investigations were performed on powders prepared by the gentle grinding of bulk samples followed by deposition onto holey carbon support films. Here a 5 wt.% SiC co-doped sample was selected, due to the excellent J_c performance in low fields. While further investigation of sectioned bulk samples is required to fully characterise the distributions of minor phases, including Mg_2Si, MgO and unreacted SiC, the TEM investigations revealed that MgB_2 in the co-doped samples contained large concentrations of defects, typical of carbon-doped specimens. Furthermore, excess carbon was also present, both in the form of graphene or graphite and amorphous carbon. The TEM results obtained from the co-doped sample containing 5 wt.% SiC are shown in Figure 2. In the low magnification bright field image (Fig. 2a) the large circled area contains both MgB_2, confirmed by the electron diffraction pattern obtained from the large circled region, and either graphene or a graphitic decomposition product of the original graphene additive, as indicated by the diffraction spots

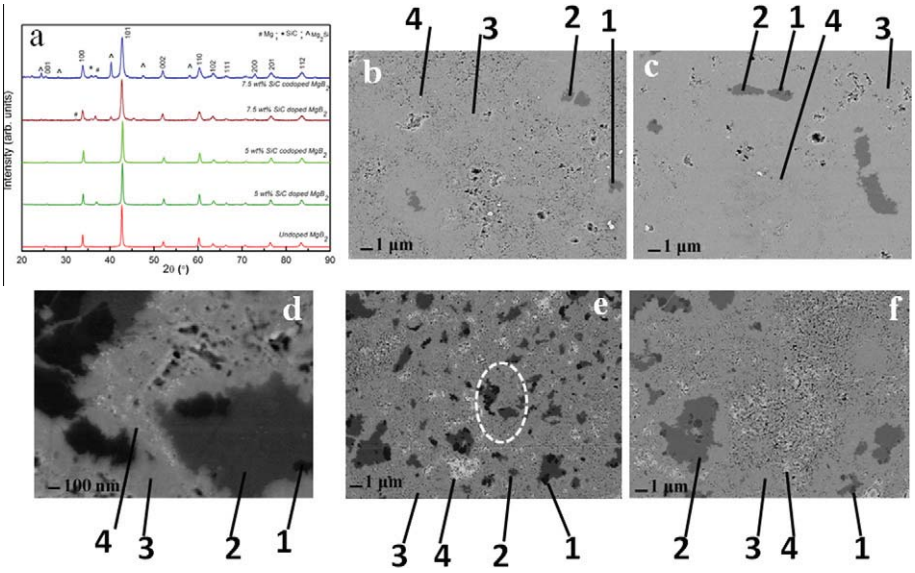

Figure 1. (a) X-ray diffraction patterns of the undoped, SiC-doped and co-doped MgB_2 bulk samples. FESEM images of: (b) 5% SiC doped, (c) co-doped 5% SiC, (e) 7.5% SiC-doped, and (f) co-doped 7.5% SiC MgB_2 bulk samples. (d) Enlarged view of the area marked in (e).

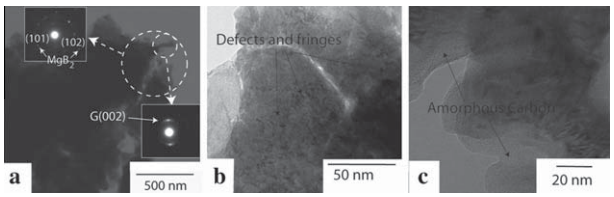

Figure 2. TEM images obtained from the 5% SiC–graphene co-doped samples. (a) A low magnification TEM image with theindicated selected area electron diffraction patterns obtained from the region believed to contain graphene or graphite plus MgB_2. (b) Bright filed contrast from MgB_2, indicating high defect densities. (c) High magnification contrast indicating the presence of significant amounts of amorphous carbon (taken from the region over a hole in the TEM support film).

associated with the small circled region. Contrast from the MgB_2 regions revealed high densities of lattice defects and fringes (Fig. 2b), which is characteristic of graphene-doped MgB_2 samples. These nanosized inclusions and lattice defects can serve as strong pinning centres to improve flux pinning. Further TEM investigations are required in order to distinguish the relative effects of carbon associated with graphene doping and carbon associated with SiC decomposition on both the MgB_2 defect structures and final microstructures of these samples. Figure 2c shows a different region of the sample, located over a hole in the sample support film. Contrast from amorphous carbon is indicated by the arrow (also confirmed by energy dispersive spectroscopy).

The critical temperature and the temperature dependence of the resistivity for all samples were analysed and are summarized in Table 1. It should be noted that the reduction in T_c due to SiC doping and co-doping at the 5 wt.% level is not significant. However, further increases in SiC doping level lead to higher levels of impurity phases associated with Mg_2Si and unreacted SiC. Dopant incorporation into the MgB_2 structure in the form of substitution of boron by carbon or the presence of additional impurities is believed to be responsible for the considerable observed drop in T_c [15].

The samples with 5 wt.% SiC doping and co-doping showed very low resistivity values, similar to the resistivity of the undoped sample, however, on increasing the SiC doping level a rapid increase in resistivity was observed. The active cross-sectional area (A_F) value of the co-doped sample with 5 wt.% SiC showed a significant improvement over the other samples. Although it is not yet fully understood, improvements in grain to grain connectivity were observed as one of the main benefits gained through graphene doping on MgB_2 [8,9]. This may be due to the presence of remaining graphene or graphitic decomposition products, as is evident in the TEM analysis, which could reside between grains, resulting in greater connectivity [9]. According to Rowel [12] factors such as porosity, density and the presence of impurities in the grains or on the grain boundaries need to be considered, as some factors affect the inter-grain connectivity while others affect the resistivity of the grains themselves, which ultimately affects the resistivity of the sample. Carbon substitution at boron sites increases the resistivity due to increased electron scattering and disorder. Doped and co-doped samples containing 5 wt.% SiC show better homogeneity, compared with 7.5 wt.% SiC-doped and co-doped samples, due to the low levels of secondary phases such as Mg_2Si and unreacted SiC, which reflect better grain connectivity, as is evident from the XRD analysis, FESEM images and A_F values. However, with increasing doping level higher resistivities were observed in the doped samples, due to both inferior grain connectivity and the higher carbon substitution. The presence of non-superconducting phases such as Mg_2Si and SiC leads to a shortened electron mean free path l, resulting in a reduced coherence length ε according to the equation $1/\varepsilon = 1/l + 1/\varepsilon_0$ [16]. The residual resistivity ratio (RRR) gives a clue to the reduction in crystallinity or increased disorder, therefore decreased values of RRR for the doped samples compared with the undoped ones reflects the effect of doping on the disorder of the samples [17].

Figure 3 shows the in-field J_c performance at 5 and 20 K for undoped, SiC-doped and co-doped bulk samples of MgB_2. The J_c curves for the co-doped samples show a significant improvement over the undoped and doped samples at both 5 and 20 K. In a zero field (20 K) the sample co-doped with graphene and 5 wt.% SiC showed a quite high critical current density value of 5.77×10^5 A cm^{-2}, and showed a 40% improvement compared with the undoped sample. It should be noted that the reduction in T_c for this sample was less than 1 K, compared with the undoped sample. The enhancement in J_c in a zero field can mainly be attributed to good connectivity. According to the resistivity analysis this sample exhibits the highest value of A_F, indicating an excellent grain to grain connectivity. The sample co-doped with graphene and 7.5 wt.% SiC shows a remarkable value of J_c, 2.08×10^4 A cm^{-2} at 5 K and 8 T, which is similar to the highest J_c ever reported for bulk samples [6]. This is a nearly 46 times improvement compared with the undoped sample. The high level of carbon substitution at boron sites and the presence of a nano-sized Mg_2Si impurity phase significantly improved J_c in high fields, by enhancing H_{c2} and flux pinning (see Fig. 1d).

The temperature dependence of the upper critical (H_{c2}) and irreversibility (H_{irr}) fields are shown in the Figure 4. It can be seen that both H_{c2} and H_{irr} increased dramatically in all doped samples, compared with the undoped samples. The highest improvement in critical field was observed in the co-doped sample with 7.5 wt.% SiC. Such an improvement in the critical field was gained due to several reasons, such as (i) C substitu-

Table 1. Critical temperature (T_c), resistivity at 40 and 300 K, residual resistivity ratio (RRR), and active cross-section (A_F) of undoped, SiC-doped and co-doped MgB_2 bulk samples.

SiC doping level (wt.%)	T_c (K)	ρ (μΩ cm)		RRR	A_F
		300 K	40 K		
0	38.87	46.65	12.74	3.65	0.126
5	38.13	40.20	12.80	3.14	0.157
5 + G	38.12	38.18	12.40	3.07	0.167
7.5	36.10	83.66	52.12	1.60	0.136
7.5 + G	35.60	87.00	52.00	1.67	0.122

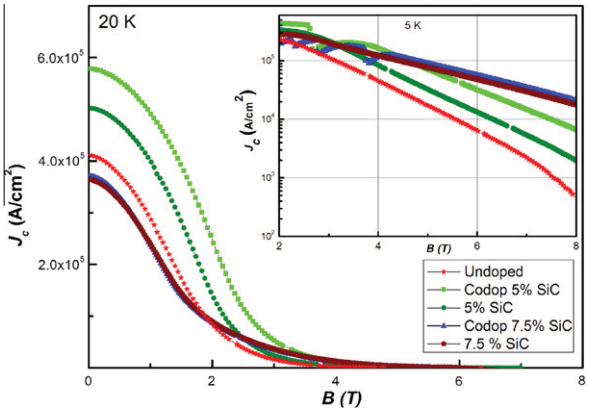

Figure 3. In-field J_c performance at 20 K for undoped, SiC-doped and co-doped MgB_2 bulk samples. (Inset) The same at 5 K on a logarithmic scale.

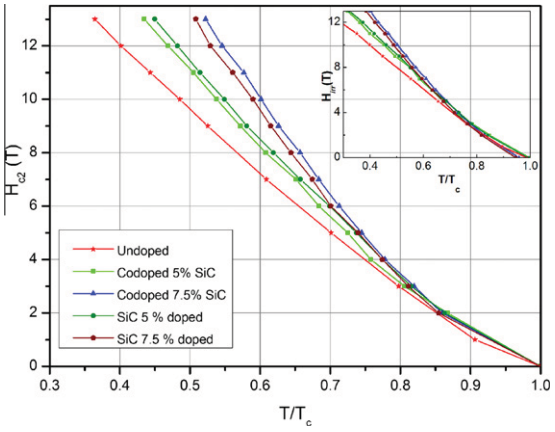

Figure 4. Normalized temperature dependence of the upper critical field H_{c2} for undoped, SiC-doped and co-doped MgB_2 bulk samples. (Inset) Normalized temperature dependence of the irreversibility field H_{irr} of the same samples.

tion for B sites, which results in an increase in intraband scattering, (ii) the formation of nano-domain structure, and (iii) the formation of a Mg_2Si impurity phase [18].

The effects of co-doping with graphene and nano-SiC with MgB_2 were systematically investigated. A significant improvement in critical current density in low fields was observed in the sample co-doped with graphene and 5 wt.% SiC, with only a small depression in T_c. This indicates that inter-grain connectivity was the dominant factor governing the performance of J_c in zero fields, while high H_{c2} and flux pinning govern the J_c performance in high fields in graphene and nano-SiC with MgB_2 bulk samples. By combining the advantages of strong flux pinning with SiC doping and good connectivity with grapheme doping co-doping is a novel approach that can be used to improve the superconducting properties in both low and high fields.

This research was performed with the support of the Australian Research Council (ARC) through project LP0989352. The authors would like to thank Dr S. Gambir and G.G. Wallace for providing graphene for this study, and P. Shamba, O. Shcherbakova, and W.X. Li for their helpful discussions. This work was supported by Hyper Tech Research Inc., OH, and the University of Wollongong.

[1] S.X. Dou, O. Shcherbakova, W.K. Yeoh, J.H. Kim, S. Soltanian, X.L. Wang, C. Senatore, R. Flukiger, M. Dhalle, O. Husnjak, E. Babic, Physical Review Letters 98 (2007) 097002.
[2] Y. Ma, X. Zhang, G. Nishijima, K. Watanabe, S. Awaji, X. Bai, Applied Physics Letters 88 (2006) 072502.
[3] R.H.T. Wilke, S.L. Bud'ko, P.C. Canfield, D.K. Finnemore, R.J. Suplinskas, S.T. Hannahs, Physical Review Letters 92 (2004) 217003.
[4] A. Serquis et al., Superconductor Science and Technology 20 (2007) L12.
[5] C. Shekhar, R. Giri, R.S. Tiwari, O.N. Srivastava, S.K. Malik, Journal of Applied Physics 102 (2007) 093910.
[6] J.H. Kim, S. Zhou, M.S.A. Hossain, A.V. Pan, S.X. Dou, Applied Physics Letters 89 (2006) 142505.
[7] X. Xu, X.L. Wang, S.X. Dou, J.H. Kim, M. Choucair, W.K. Yeoh, R.K. Zheng, S.P. Ringer, Superconductor Science and Technology 23 (2010) 085003.
[8] K.S.B. De Silva, X. Xu, S. Gambhir, X.L. Wang, W.X. Li, G.G. Wallace, S.X. Dou, Scripta Materialia 65 (2011) 634.
[9] K.S.B. De Silva, S. Gambir, X.L. Wang, X. Xu, W.X. Li, D.L. Officer, D. Wexler, G.G. Wallace, S.X. Dou, Journal of Materials Chemistry 22 (2012) 13941.
[10] K.S.B. De Silva, X. Xu, W.X. Li, Y. Zhang, M. Rindfleisch, M. Tomsic, IEEE Transactions on Applied Superconductivity 21 (3) (2011) 2686.
[11] C.P. Bean, Reviews of Modern Physics 36 (1964) 31.
[12] J.M. Rowell, Superconductor Science and Technology 16 (2003) R17.
[13] S.X. Dou, A.V. Pan, S. Zhou, M. Ionescu, X.L. Wang, J. Horvat, H.K. Liu, P.R. Munroe, Journal of Applied Physics 94 (2003) 1850.
[14] B. Birajdar, O. Eibl, Journal of Applied Physics 105 (2009) 033903.
[15] Z. Xianping et al., Superconductor Science and Technology 19 (2006) 479.
[16] A. Yamamoto, J. Shimoyama, S. Ueda, Y. Katsura, I. Iwayama, S. Horii, K. Kishio, Applied Physics Letters 86 (2005) 212502.
[17] X.-L. Wang, S.X. Dou, M.S.A. Hossain, Z.X. Cheng, X.Z. Liao, S.R. Ghorbani, Q.W. Yao, J.H. Kim, T. Silver, Physical Review B 81 (2010) 224514.
[18] O.V. Shcherbakova, A.V. Pan, S.X. Dou, Manesium Diboride Supercoductors Development and Properties, first ed., VDM Verlagand, Saarbrücken, Germany, 2009.